ALLEN INSTITUTE for BRAIN SCIENCE
Fueling Discovery

Allen Mouse Common Coordinate Framework

TECHNICAL WHITE PAPER:
ALLEN MOUSE COMMON COORDINATE FRAMEWORK

OVERVIEW

The Allen Mouse Common Coordinate Framework (CCF) is an essential tool to understand the structure and function of the mouse brain at molecular, cellular, system and behavioral levels. It has been successfully used for large-scale data mapping, quantification, presentation, and analysis and has evolved through the creation of multiple versions. The first version (in 2005) of the CCF was created to support the product goals of the Allen Mouse Brain Atlas (**Figure 1**) (Lein *et al*., 2007). The framework was based upon the Allen Reference Atlas (ARA) specimen (Dong, 2008) in which a 3-D volume was reconstructed using 528 Nissl sections of a near complete brain. Approximately 200 structures were extracted from the 2-D atlas drawings to create 3-D annotations. A second version (in 2011) of a refined CCF was constructed to support the scientific objectives of the Allen Mouse Brain Connectivity Atlas (Oh *et al*., 2014) where a double-sided and more deeply annotated framework was needed (**Figure 1**). During the development, flaws in the 3-D reconstructions were corrected and the volume was mirrored across the mid-line to create a symmetric space. Eight hundred and sixty structures were extracted and interpolated to create symmetric 3-D annotations.

In 2012, the Institute launched a 10 year plan to investigate how the brain works that includes cataloguing different kinds of individual cells in the brain, understanding the relationships between those different kinds of cells, comprehending how information is encoded and decoded by the brain, and modeling how the entire brain processes and computes information. To facilitate this effort, a next generation CCF was needed to support integration of data generated as part of this plan. Version 3 (v3) of the CCF is based on a 3-D 10µm isotropic, highly detailed population average of 1675 specimens. Currently, CCF v3 consists of 185 newly drawn structures in 3-D: 123 subcortical structures, 41 fiber tracts (plus ventricular systems), and 21 cortical regions including primary visual and higher visual areas. The final product of CCF will consist of ~300 gray matter structures, cortical layers, ~80 fiber tracts, and ventricle structures in 3-D. The ARA ontology (Dong 2008) was utilized in the annotation and updated to include higher visual areas.

Newly drawn structures currently span 50% of the brain, thus structures from CCF version 2 (v2) were used to create a completed interim map to support the whole brain quantification needed for the Allen Mouse Brain Connectivity Atlas. The 3-D annotation and Nissl volume from CCF v2 were deformably registered to the anatomical template of v3. Structures targeted for the final product of the CCF that have not yet been drawn were extracted from v2 and merged with v3. The interface between old and new structures were manually inspected and filled to create smooth transitions.

The maintain product continuity, whole brain quantification and visualization for the Allen Mouse Brain Atlas (gene expression) will use the registered Nissl and CCF v2 (ARA) annotations.

This technical white paper describes the methods used to generate the CCF v3, including the creation of the anatomical template, reference data sets, new and updated structures, and 3-D annotation and processing.

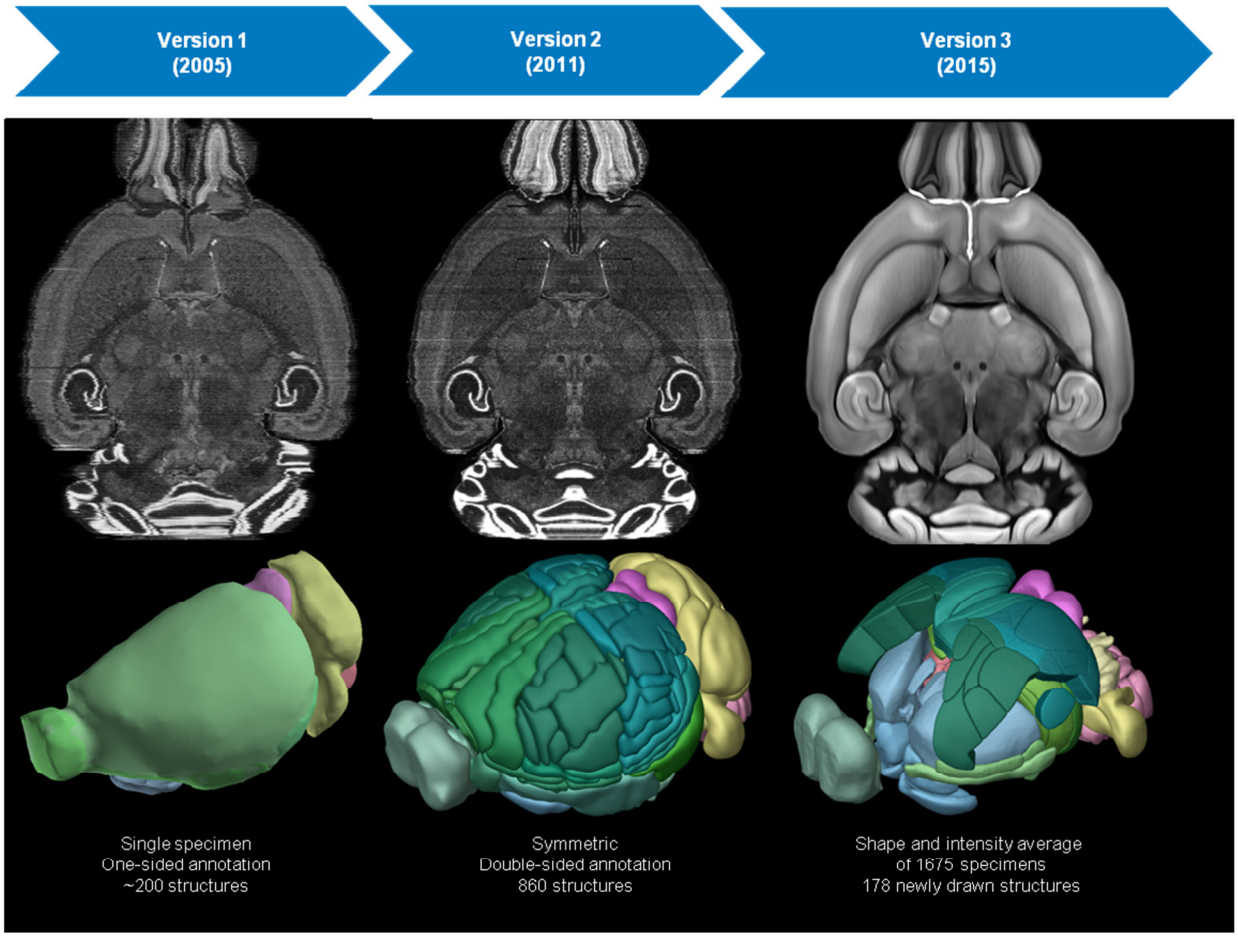

Figure 1. Evolution of the Allen Mouse Common Coordinate Framework.
The first version (2005) supported the Allen Mouse Brain Atlas and was based upon the Allen Reference Atlas specimen. A second version (2011) supported the Allen Mouse Brain Connectivity Atlas where a double-sided and more deeply annotated framework was needed. Version 3 (2015) of the Common Coordinate Framework is based on a population average of 1675 specimens and has 178 newly drawn 3-D structures, including nine higher visual areas.

CREATION OF THE ANATOMICAL TEMPLATE

The anatomical template of CCF v3 is a shape and background signal intensity average of 1675 specimens from the Allen Mouse Brain Connectivity Atlas (Oh *et al*., 2014). Specimens in the Allen Mouse Brain Connectivity Atlas were imaged using a customized serial two-photon (STP) tomography system, which couples high-speed two-photon microscopy with automated vibratome sectioning. STP tomography yields a series of inherently prealigned images amenable for precise 3-D spatial mapping.

A population average was created through an iterative process, averaging many brains over multiple cycles. This iterative process was bootstrapped by 12-parameter affine registration of specimens to the "registration template" created as part of the Allen Mouse Brain Connectivity Atlas data processing pipeline (Kuan *et al*. 2015). The "registration template" effectively provides initial orientation and size information to this process. To create a symmetric average, each of the 1675 specimens was flipped across the mid-sagittal plane and the flipped specimens were used as additional input to the averaging process. The total 3350 (= 2 x 1675) hemispheres were registered and averaged to create the first iteration of the CCF v3 anatomical template.

Following the method in (Fonov 2011), two steps were performed during each iteration: (1) each specimen was deformably registered to the template and averaged together; (2) the average deformation field over all specimens was computed, inverted, and used to deform the average image created in (1). This shaped

normalized average was then used as the anatomical template in the next iteration. This algorithm continues until the mean magnitude of the average deformation field was below a certain threshold. For computational efficiency, the method was first applied to the data down sampled to 50µm resolution until convergence was reached. This result was then used as input to the 25µm processing round. In the final step, the specimens were resampled at 10µm resolution and averaged to create the final 3-D volume.

The anatomical template possesses two properties: (a) the intensity difference between the average and each transformed specimen was minimized and (b) the magnitude of all the deformation fields used to transform each specimen was minimized. The anatomical template is thus the average shape and average appearance of the population of 1675 specimens and shows remarkably clear anatomic features and boundaries for many brain structures.

REFERENCE DATA SETS

Reference data sets are crucial for confirming the identification of anatomical structures visible in the anatomical template and also for drawing those that are not visible in the anatomical template. The following were used to delineate gray matter and white matter structures in 3-D.

1. **Allen Mouse Brain Connectivity Atlas - Projection Data** (connectivity.brain-map.org): This data set shows the projections and projection topographies from given anatomical structures. Methods for data generation have been previously described in detail (Oh *et al*., 2014) and can be found in the Technical White Papers located in the Documentation tab. STP tomography imaging enables accurate registration of the data to the CCF.

2. **Allen Mouse Brain Connectivity Atlas - Reference Data** (connectivity.brain-map.org): Reference data includes two histology datasets (Nissl- and AChE-stained specimens) and three immunohistochemistry datasets (SMI-32 and Parvalbumin, NeuN and NF-160, calbindin 1 and SMI-99 double-stained specimens). See the Reference Dataset white paper located in the Documentation tab for more details. Reference data were registered to the CCF using customized methods. Registration accuracy was limited due to the modest amount of deformation and tissue damage. Regardless, these datasets have great utility in providing anatomical details for delineating certain structures.

3. **Transgenic Mouse Data** (data not published): Transgenic mouse brains that exhibit differential tdTomato labeling in genetically-defined cell types are important tools for anatomic delineation, particularly where structures and their borders cannot be distinguished using the anatomical template. For this version of the CCF, two datasets using transgenic mouse brains generated by the same perfusion and imaging procedures as in the Allen Mouse Connectivity Atlas were used, allowing easy integration of the data to the CCF. An additional 28 transgenic lines will be used to provide anatomical information for completing the targeted 3-D structural delineation for the final product.

4. **ISH Data** (mouse.brain-map.org): Molecular markers have been a powerful tool for the delineation of brain structures (Lein *et al*., 2005; Lein *et al*., 2007; Dong, 2008). There are a number of genes that exhibit remarkably regionalized expression that were used to indicate borders in the anatomical template as well as confirm those previously delineated.

UPDATED AND NEW STRUCTURES

The ARA anatomical ontology was used for the CCF to maintain continuity for multiple products that are part of the Allen Brain Atlas Data Portal. Updates to the ARA ontology were made that included the addition of structures in the higher visual areas, specifically the anterior visual area (layers 1, 2/3, 4, 5, 6a, and 6b), lateralintermediate area (layers 1, 2/3, 4, 5, 6a, and 6b), rostrolateral visual area (layers 1, 2/3, 4, 5, 6a, and 6b), and postrhinal area (layers 1, 2/3, 4, 5, 6a, and 6b) to the visual and posterior parietal area branches of the brain structure tree.

Structures drawn in 3-D were located throughout the brain, including in the isocortex (21 structures), olfactory areas (5 structures), hippocampal formation (8 structures), cortical subplate (5 structures), striatum (5 structures), pallidum (3 structures), thalamus (33 structures), hypothalamus (6 structures), midbrain (16 structures), pons (12 structures), medulla (25 structures), cerebellum (5 structures), fiber tracts (35 structures), and ventricular systems (6 structures). A detailed structure list is shown in **Table 1**.

3-D ANNOTATION AND PROCESSING

3-D Annotation

For the 3-D annotation, manual delineation of the anatomical template was a combined process of structure discovery and 3-D illustration carried out at various levels: as individual structures, group of local structures and interface between groups (**Figure 2A**). Using anatomical template contrast features and fiducials from select supporting data (described below), structures were landmarked, filled-in serially, and validated. In certain cases the process was modified to include previously-drawn structures (**Figure 2B**), which greatly increased anatomic accuracy and illustrative efficiency. Once a critical mass of content was reached, a global merging of all individual and local structure groups was performed (**Figure 2C**). At this stage, local phenomena such as overlaps and gaps were considered at a brain-wide level and brought into alignment. Structures previously deferred on the basis of "negative space" considerations were defined and illustrated here as well. The process was completed by a final evaluation of structures in the component 2-D plates as well as the rendered 3-D composition.

ITK-SNAP (www.itksnap.org) a freeware 3-D annotation tool (Yushkevich *et al.*, 2006) was utilized throughout the discovery and illustration processes. After loading the 10µm/voxel anatomical template, a region of interest (ROI) was identified provisionally in the given viewing planes (horizontal, sagittal, and coronal) by the chief neuroanatomist. Key anatomical features present in the template were observed, researched, and visually enhanced by the standardized employment of image adjustment tools provided in ITK-SNAP. When additional evidence was necessary and available, supporting data was registered and overlaid semi-transparently or launched in a parallel ITK-SNAP window for voxel-to-voxel tracking. Once an ROI was thoroughly and satisfactorily evaluated, the neuroanatomist produced a landmark segmentation (multi-planar 2-D delineations at regular intervals), which was given to illustration specialists who complete the segmentation serially and refine surface features to an appropriate level of maximum smoothness. The resulting structure was then compared back to the original landmark segmentation and either refined or submitted to the chief neuroanatomist for final approval. These were the principle mechanics for building CCF structures in ITK-SNAP. As additional structures were built, specialized macros for merging and splitting individual files were utilized to facilitate group delineations and form-fitting adjustments at local and global levels, respectively.

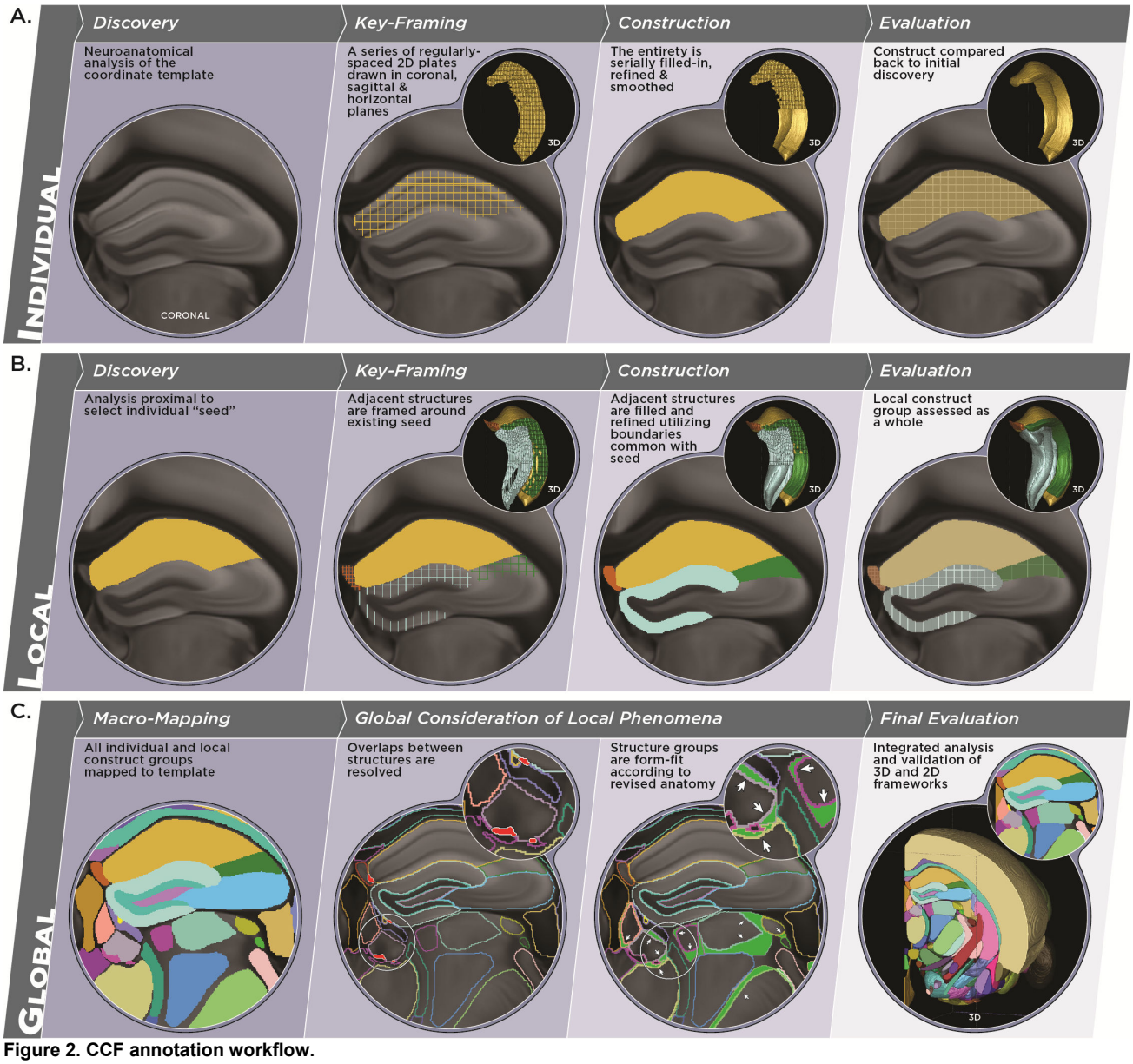

Figure 2. CCF annotation workflow.
A. Structures with sufficient individual context are identified (discovery), 3-dimensionally outlined (key-framing), filled-in (construction) and validated (evaluation). **B.** Where possible, building is then performed in direct context of individually-built structures, such as the hippocampus (shown). This aids the fill-in process and ensures seamless interlocking of the entire local structure group. **C.** After building at the individual and local levels, structures are finally brought together for negotiation in a single, brain-wide context. Once overlaps are resolved and structures appropriately form-fit, a final evaluation is performed to ensure overall accuracy in 2-D and 3-D frameworks.

Creating a Curved Cortical Coordinate System

As part of the construction of CCF v3, a curved cortical coordinate system was developed to enable the integration of information from different cortical depths. The construction started with a manual delineation of the isocortex. Definition of the isocortex used here was adapted from the ARA ontology (Dong, 2008). According to that definition, the isocortex is bordered rostroventrally by the main olfactory bulb (MOB), the accessory olfactory bulb (AOB) and the anterior olfactory nucleus (AON), laterally by the AON, the piriform area (PIR) and the entorhinal area (ENT), medially by the dorsal peduncular area (DP), the subiculum (SUB) and postsubiculum (POST), and caudally by the medial entorhinal (ENTm) area, and parasubiculum (PAR). Although the boundaries of isocortex were recognizable in the anatomical template itself, manual delineation was greatly facilitated by the addition of transgenic mouse brain data registered with the anatomical template.

In this case, calbindin expression was used (visualized by crossing the Calbindin1-2A-dgCre mouse line with the Ai14 reporter to label calbindin positive cells with tdTomato (red) fluorescent protein). Calbindin is strongly expressed throughout the isocortex, except in the ventral portion of the retrosplenial area (RSPv), and is weakly expressed in the paleocortex, including the entorhinal area (ENT) and the piriform area (PIR).

Figure 3 shows the anatomical template with overlaid reference data at select coronal levels, from rostral to caudal. Rostral isocortex (orbital area and agranular insular area) was separated from the olfactory bulb (MOB and AON) on the basis of differential fluorescent signal (**Figure 3A**). Lateral isocortex (agranular insular area and perirhinal area) was separated from the AON, PIR, and ENT in a similar fashion (**Figure 3 A-D**). Compared to the lateral isocortex, medial isocortex has strong fluorescent signal only in the rostral part. Rostromedial isocortex (infralimbic area) was also separated from dorsal peduncular areas (DP) by fluorescent signal differences (**Figure 3B**). For the caudomedial portion of isocortex (RSPv), separation from SUB and POST was indicated by dramatic laminar differences observed in the anatomical template itself (**Figure 3D**). Fluorescence differences were again used in the caudal part of the isocortex (posterolateral visual area and RSPd) for separation with ENTm and PAR.

After the borders of isocortex were defined, Laplace's equation was solved between pia and white matter surfaces resulting in intermediate equi-potential surfaces (**Figure 4A**). Streamlines were computed by finding orthogonal (steepest descent) path through the equi-potential field (**Figure 4B**). Information at different cortical depths can then be projected along the streamlines to allow integration or comparison. Streamlines were used to facilitate the annotation of higher visual areas and related cortical areas.

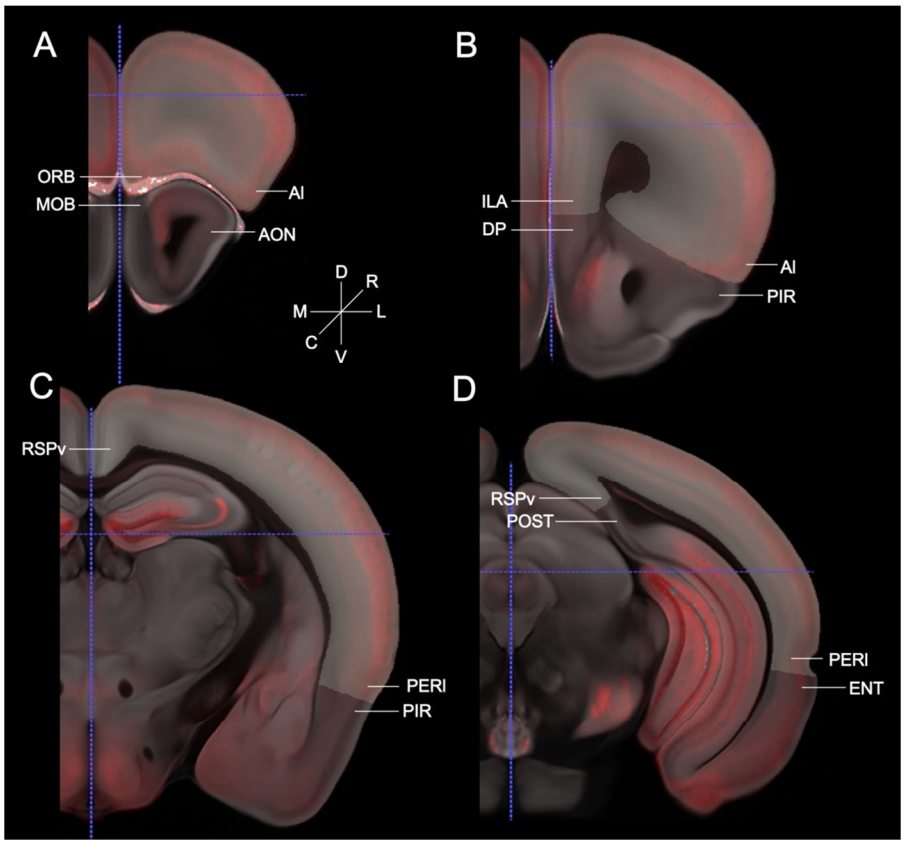

Figure 3. Delineation of the isocortex.
The transgenic reference data (Calbindin1-2A-dgCre) were overlaid with the anatomical template. Structures expressing tdTomato (a red fluorescent protein) were labeled in red. **A-D.** Examples show the boundaries of the isocortex at different levels from rostral to caudal. The border of the isocortex was indicated by sticks and the isocortex was painted in light yellow. Abbreviations: AI, agranular insular area; AON, anterior olfactory nucleus; C, caudal; D, dorsal; DP, peduncular area; ENT, entorhinal area; ILA, infralimbic area; L, lateral; M, medial; MOB, main olfactory bulb; ORB, orbital frontal area; PERI, perirhinal area; PIR, piriform area; POST, postsubicullum; R, rostral; RSPv, ventral part of the retrosplenial area; V, ventral.

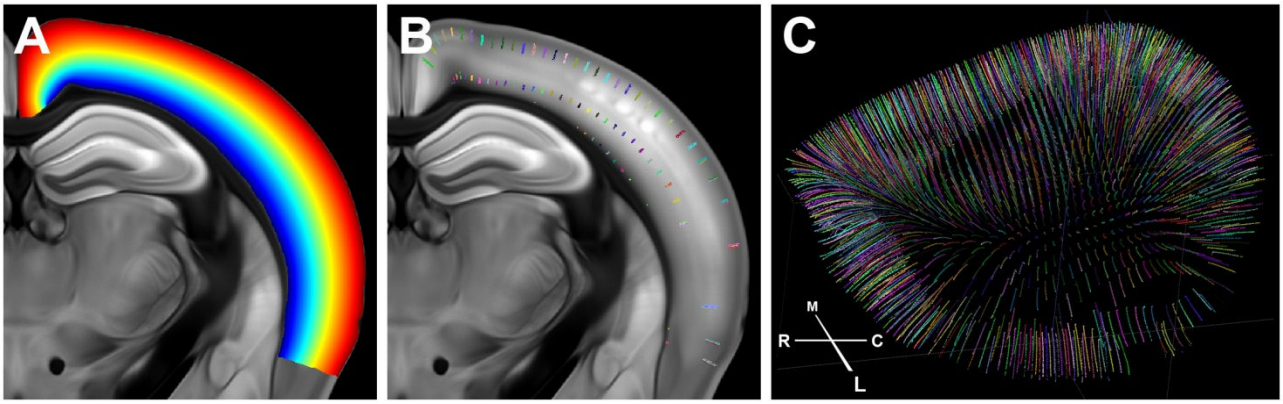

Figure 4. Curved cortical coordinate system.
A. Laplace's equation is solved between pia and white matter surfaces to generated intermediate equi-potential surfaces as analog to cortical depth. **B-C**. Streamlines are computed by finding a curved "orthogonal" path through the equi-potential field.

Higher Visual Areas

In the ARA (Dong, 2008), the visual cortex consists of six visual areas drawn on a single, Nissl-stained specimen. Recent studies using tract-tracing and intrinsic signal imaging methods (Wang and Burkhalter, 2007; Marshel *et al*., 2011; Garrett *et al*., 2014) have shown however, that there are at least ten visual areas that contain complete visuotopic maps. These studies use flattened cortex surface views to exhibit distinguishable topographies of higher visual areas. Since higher visual areas are impossible to distinguish in the anatomical template itself (**Figure 5A**), a similar surface-guided strategy was sought for the delineation of the higher visual areas for the CCF.

Since different angles provide different information regarding surface views, five angles were chosen to cover the full extent of visual cortex and its closely related areas: top, rotated, medial, back, and side. An example, top view, is shown in **Figure 5**. To generated surface views of the anatomical template, the highest intensity (brightest) voxel along a streamline was projected to its surface voxel. Additional reference data can be incorporated into the surface views by registering the data into the CCF and similarly projecting maximum intensity information to the surface using the streamlines.

Inspection of the anatomical template surface view revealed distinctly bright domains putatively representing the primary visual, somatosensory and auditory areas, and the retrosplenial area (**Figure 5A**). Overlaying of SMI-32 stained reference data, a neurofilament antibody assay previously reported to stain heavily in these regions (Wang et al., 2011), confirmed their presence and location, which were landmarked (**Figure 5B**). The darker regions between four landmarked areas contain higher visual areas.

To reveal higher visual areas, 26 injections located throughout retinotopic space in primary visual area were selected from the Allen Mouse Brain Connectivity Atlas. Images for each of the 26 injections were segmented and registered (Kuan *et al*., 2015) to obtain 3-D volumes of projection signal density. The 26 density volumes were combined to create a color-coded weighted source location map. For each injection, a "center" 3-D location was computed. At each voxel on the 3-D map, a weighted source location was computed as the weighted sum of injection center locations with the weights being the projection density value at the voxel arising from each of the different injections. Additionally, summed projection density over all injections was also computed for each voxel. To create a surface view, only signal within 0.1 to 0.5 normalized cortical depth was considered. The maximum summed projection density voxel for each streamline was identified and the weighted source location of the maximum density voxel was projected to the surface. To aid visualization, a weighted location was color-coded as follows: the HSV (hue-saturation-value) color wheel was embedded into primary visual area such that magenta corresponds to the nasal visual field, cyan for temporal visual field and blue for lower visual field. Color at any intermediate location was interpolated from the HSV formula. A color-

coded top view is shown in **Figure 5C**. This result recapitulates the previous finding in which higher visual areas were delineated based on their visuotopic maps (Wang and Burkhalter, 2007).

In addition to visuotopic maps, a virtual callosal projection pattern was generated using cortical injection data from the Allen Mouse Brain Connectivity Atlas. A virtual callosal map was created using 108 injections spanning the isocortex. A max projection density map was created by finding, at each voxel, the maximum density value over all injections. Since all injections in the Allen Mouse Brain Connectivity Atlas were in the right hemisphere, to create a callosal map, each dataset was flipped across mid-sagittal plane and treated as virtual left hemisphere injections. A surface view was then generated by considering only signal within 0.1 to 0.5 normalized cortical depth and projecting the largest maximum value to the surface. This projection pattern was employed for fixed landmark referencing, which is important because higher visual areas have unique spatial relationships with callosal projections from the opposite hemisphere. As shown in **Figure 5D**, callosal projections terminate at the borders between the primary visual area and the lateral and anterolateral visual areas, and at the border between the primary somatosensory area and the supplemental somatosensory area, while avoiding the rest of the primary visual area and barrel fields of the primary somatosensory area. A large acallosal zone is located on the lateral side of the primary visual area and a small acallosal ring is located rostrolateral to the primary visual area and caudal to the primary somatosensory cortex. Overall, this surface callosal projection pattern is similar to what has been shown in flattened cortex (Wang and Burkhalter, 2007). **Figure 5E** shows that overlaying virtual callosal projections with the anatomical template further restrict boundaries of the higher visual areas.

Based on topography and the relationship to callosal projections, individual higher visual areas were drawn from surface views. In **Figure 5**, the lateral visual area located in the caudal part of the large acallosal zone on the lateral side of the primary visual area has a visuotopic map that mirrors the primary visual area. The lateral intermediate area on the lateral side of the lateral visual area and on the caudal side of the anterolateral visual area, which falls in the caudolateral part of the large acallosal zone, has a visuotopic map that mirrors the lateral visual area. The postrhinal area, which falls in the callosally labeled region, has a visuotopic map that mirrors the posterolateral visual area located caudally to the lateral and primary visual areas. The anterolateral visual area, which falls in the rostral part of the large acallosal zone on the rostrolateral side of the primary visual area, has a visuotopic map that mirrors the lateral visual area. The rostrolateral visual area located between the rostrolateral part of the primary visual area and the caudal part of the primary somatosensory area has a visuotopic map that mirrors the anterolateral visual area. The visuotopic map of the anteromedial visual area is a mirror image of the posteromedial visual area.

It is noteworthy that the anterior visual area receives weaker input from the primary visual area compared to other higher visual areas and its visuotopic map is coarse. The boundary of the anterior visual area was drawn between the rostrolateral and the anteromedial visual areas mediolaterally and between the rostral tip of the primary visual areas and the caudal part of the primary somatosensory area rostrocaudally. In total, nine higher visual areas were drawn from the surface views. These 2-D surface drawings were transformed into 3-D by extrapolating surface annotation into the 3-D isocortex by copying the annotation along the streamlines (**Figure 1**).

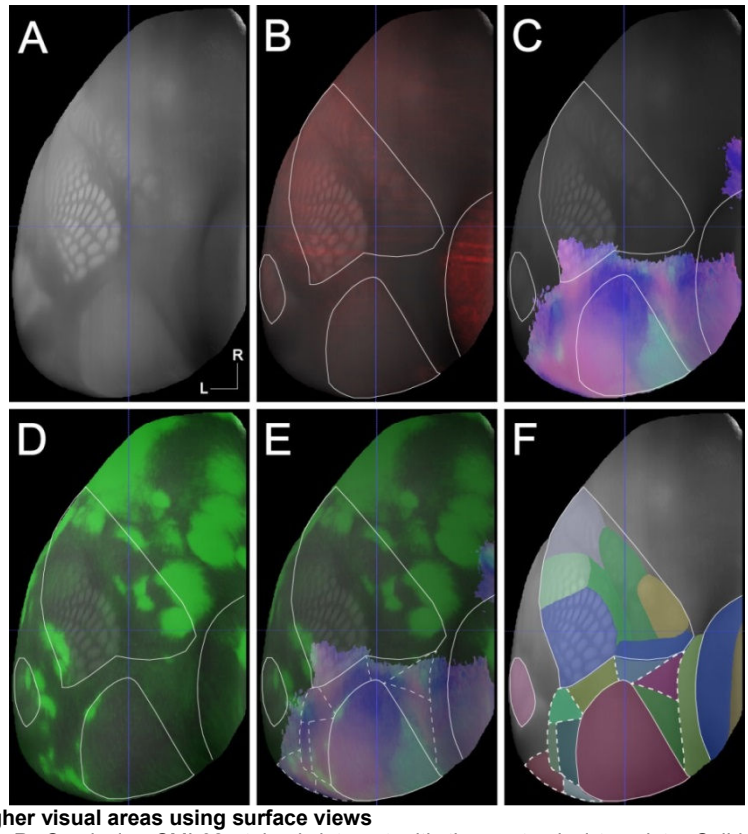

Figure 5. Delineation of higher visual areas using surface views
A. The anatomical template. **B.** Overlaying SMI-32 stained data set with the anatomical template. Solid lines indicate borders of the primary visual area, primary somatosensory area, primary auditory area, and retrosplenial area. **C.** Composite visuotopic maps of striate and extrastriate visual areas. **D.** Virtual callosal projections. **E.** Overlaying visuotopic maps and virtual callosal projections with the anatomical template. Dashed lines indicate the borders of the higher visual areas. **F.** Higher visual areas and their closely-related cortical areas (color coded). Abbreviations: R, rostral; L, lateral.

White Matter Tracts and Ventricles

The delineation of white matter (WM) tracts was made on the basis of inherent contrast features in the anatomical template in combination with myelin basic protein (SMI-99), neurofilaments (SMI-32 and NF-160), parvalbumin (PV), and calbindin (CB) reference stains. Although WM tracts generally exhibited lower signal intensity (darker) than gray matter structures (brighter) in the anatomical template, these features were not necessarily homogenous between different WM tracts or along individual WM tracts themselves. In the case of isolated and solid WM bundles such as anterior commissure, fornix, fasciculus retroflexus, and mammilothalamic tract, contours and trajectories were easily defined without the need of additional data.

In most other cases, however, WM tracts adjoined, merged (mix) or intersected other bundles and/or portions of gray matter structures at particular locations, leading to complex signal intensities along their paths, thus necessitating the correlation of template signal intensity with reference data for accurate delineation of boundaries and trajectories. For example, the medial lemniscus travels through the medulla, pons, and midbrain on its way to the thalamus, exhibiting significant changes in shape, size, location, topography, and signal intensity throughout (**Figure 6**). Specifically, intermediate intensity (medium-dark) was seen in the thalamus (**Figure 6A**) and upper midbrain (**Figure 6B**), low intensity (dark) was seen in the lower midbrain (**Figure 6C**), high intensity (least dark) in the upper pons (**Figure 6D**), and low intensity (dark) in the lower pons (**Figure 6E**) and medulla (**Figure 6F**). The trajectory and contour of the medial lemniscus was confirmed by analysis of sequential PV-stained sections, which revealed strong staining and a distinct fiber orientation pattern (green in **Figure 6A'- 6F'**). It is important to note that the medial lemniscus adjoins the cerebral peduncle (cpd) in the lower midbrain (**Figure 6C**), mixes in the upper pons with other fibers, which are PV-negative and SMI-32 positive (red in **Figure 6D**), and is crossed in the lower pons by the trapezoid body (tb), which is PV-positive but runs in a transverse direction (green in **Figure 6E**). In the medulla, the medial

lemniscus is located dorsal to the pyramidal tract (py), which is negative in both PV and SMI-32 stains (**Figure 6F**).

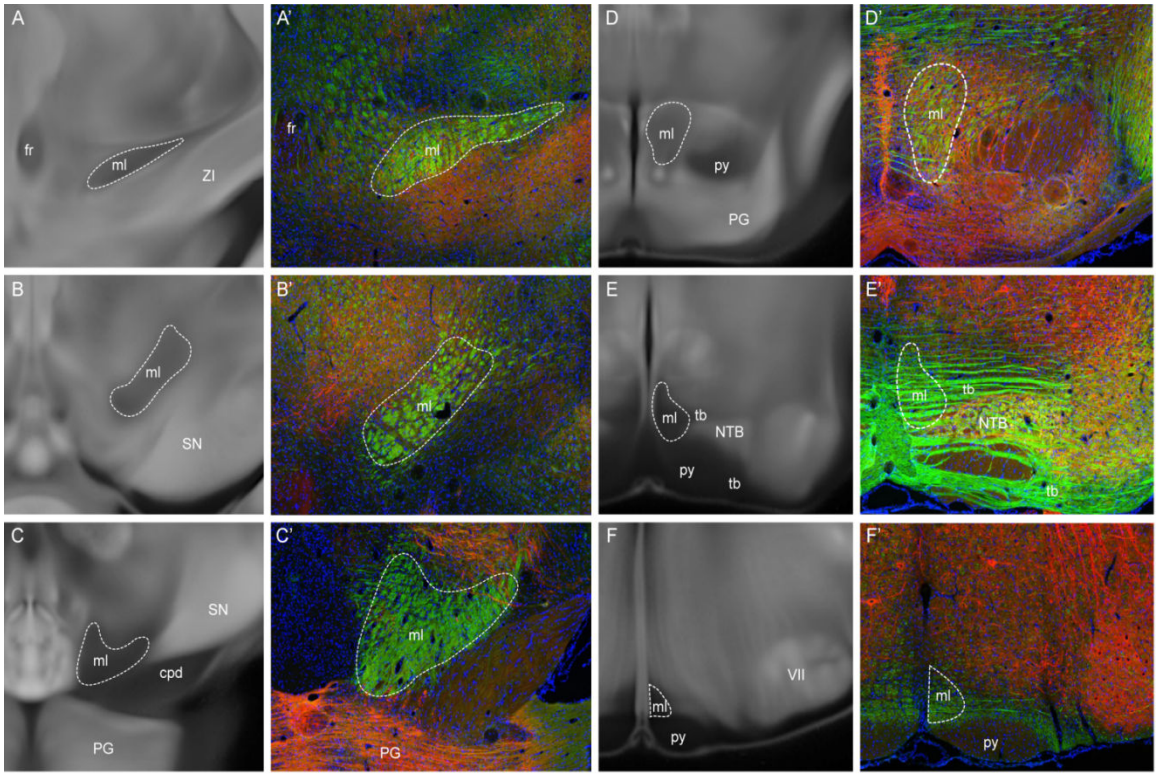

Figure 6. Changes in location, shape, size, topography and signal intensity of the medial lemniscus (ml) along its trajectory and the usefulness of reference data in delineation of white matter tracts.
A-F. Rostral–caudal template images containing the medial lemniscus and adjoining structures. **A'-F'.** Double-stained sections at the levels **A-F** showing PV- (green) and SMI-32- (red) stained gray and white matter structures. These sections were also counterstained with DAPI (blue). Abbreviations: ZI, zona incerta; fr, fasciculus retroflexus; SN, substantia nigra; cpd, cerebral peduncle; PG, pontine gray; py, pyramid; tb, trapezoid body; NTB, nucleus of the trapezoid body; VII, facial motor nucleus.

In certain cases other stains were used, as were tracer experiments from the Allen Mouse Brain Connectivity Atlas. Allen Mouse Brain Connectivity Atlas data (Oh *et al*., 2014) was especially useful when the anterograde tracer (rAAV) was injected in a desired anatomic structure restrictively (*e.g.* red nucleus). In this scenario, trajectories of a fiber bundle (*e.g.* rubrospinal tract originated from red nucleus) were confidently traced with modest adjustment according to contours exhibited in other reference data.

Finally, the ventricular system (lateral, third, fourth ventricles and cerebral aqueduct and central canal) was also delineated based on low signal intensity (dark) with exception in the regions occupied by the choroid plexus, which display higher signal intensity (less dark) and were included in the corresponding ventricles. The ependymal layer lining all the ventricular walls were also included in the corresponding ventricles.

Delineation of Challenging Structures
In the anatomical template, a structure that contains more and larger cells, such as the barrel fields of the primary somatosensory area, was generally brighter than one that contains less and smaller cells, such as fiber tracts. Many structures throughout the brain can be differentiated on these native contrast features, and thus delineated in 3-D (**Table 1**). While concurrent delineation in coronal, sagittal, and horizontal planes had many advantages over one plane alone (particularly in the coherency of the resulting construct), there were challenges when relying on the anatomical template alone. These challenges can be largely divided into two categories: 1) structure X is clearly visible in the anatomical template but is difficult to see in a traditional Nissl-based reference, and 2) structure X is comprised of heterogeneous cell groups or contains conspicuous

subdivisions in the anatomical template. Examples of both are shown in **Figures 7-8**, though in general the latter was encountered more frequently than the former. Representing the first category is CA2 of the hippocampus. It is markedly brighter than CA1 and CA3 in the anatomical template (**Figure 7 A-C**) and extends rostrodorsally (**Figure 7 D-F**) into a region apportioned to CA3 in Paxinos and Franklin (Paxinos and Franklin, 2001) and Dong reference atlases (Dong, 2008).

To address these discrepancies and ensure that it was not simply a case of specimen variability, additional information was sought. Our delineation of CA2 is consistent with a previous study by Lein *et al*. (2005) whose 3-D reconstruction of CA1, CA2, and CA3 was based on gene expression patterns of these regions. In addition to gene expression (*Pcp4*, experiment ID *79912613*) (**Figure 7 G-I**), it was found that the connectivity data from the Allen Mouse Brain Connectivity Atlas (experiment IDs 158314987 and 182182936) (**Figure 7 J-L**) supports the 3-D drawing of CA2 as well. As confirmed by multiple data modalities, this may be the truest shape for CA2 to date.

Representing the second category is the lateral nucleus of the thalamus (LP). LP is a heterogeneous complex consisting of 5 nuclei (Paxinos and Franklin, 2001), which exhibit a differential brightness profile from dorsal to ventral and medial to lateral in the anatomical template (**Figure 8A**, **8D**, and **8G**). Because structures surrounding LP, such as the lateral dorsal nucleus of thalamus, the dorsal part of the lateral geniculate complex, the anterior pretectal nucleus, and the posterior complex of thalamus appear very distinct in the anatomical template, these were drawn first. LP was tentatively placed in the resulting 3-D negative space (**Figure 8B**, **8E**, and **8H**), and then confirmed and refined by Allen Mouse Brain Connectivity Atlas data (experiment IDs 127089669 and 100141796) (**Figure 8C**, **8F**, and **8I**). Whenever the anatomical template was not sufficient for delineation, molecular, connectivity, transgenic, and reference atlas data were then employed.

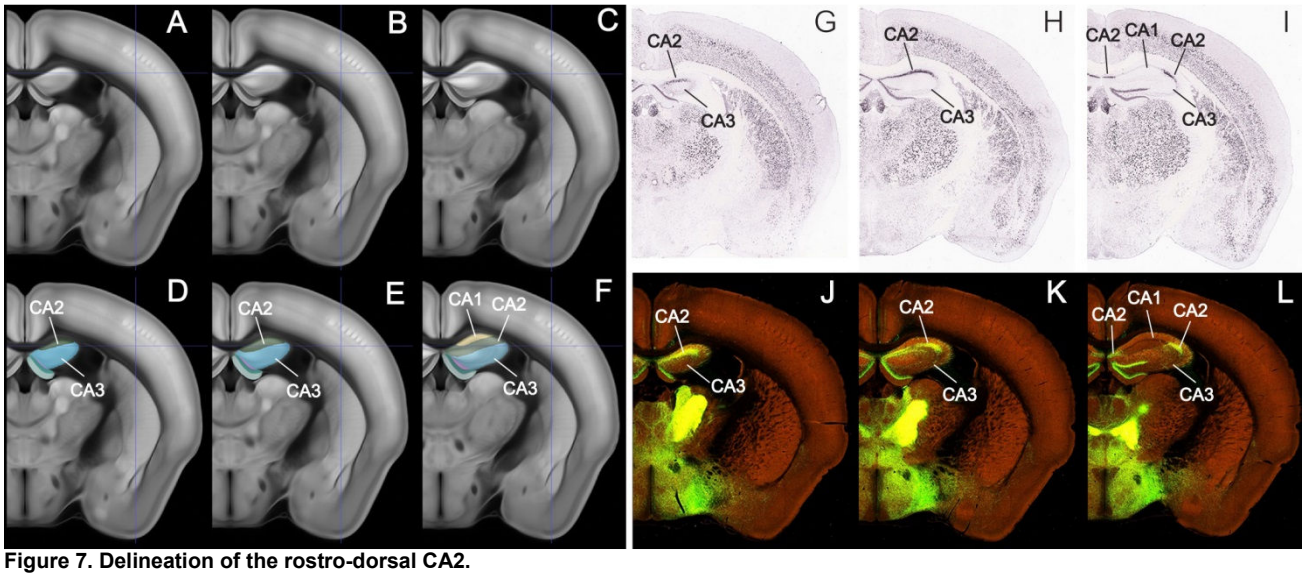

Figure 7. Delineation of the rostro-dorsal CA2.
CA2 is brighter on the anatomical template (**A, B, C**), and drawn in green (**D, E, F**), and is confirmed by gene expression from the Allen Mouse Brain Atlas (**G, H, I**) and connectivity data from the Allen Mouse Brain Connectivity Atlas (**J, K, L**).

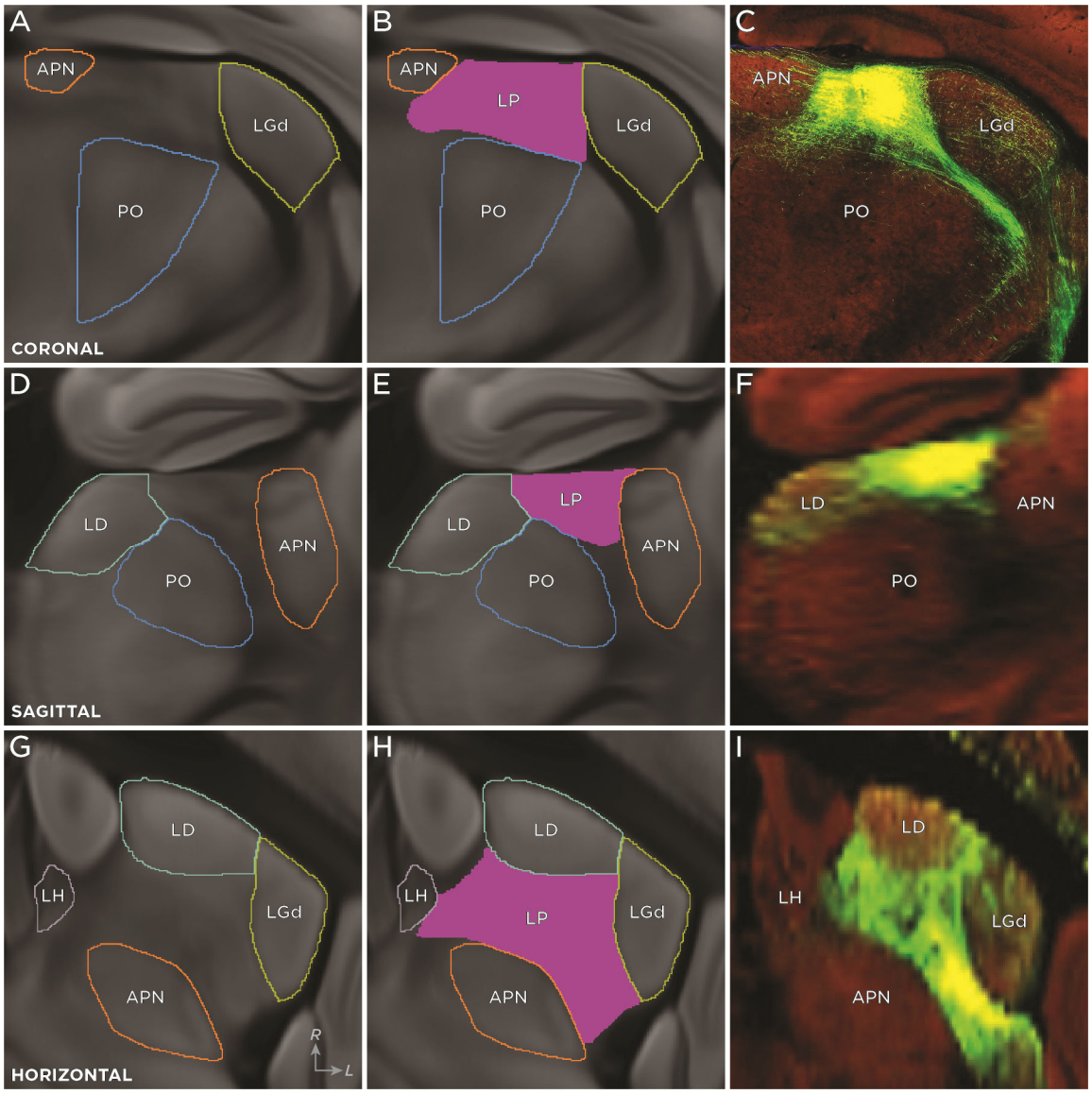

Figure 8. 3-D annotation of thalamic nucleus LP.
A, **D**, and **G** show the thalamic nucleus LP contained in coronal, sagittal, and horizontal planes. The structures surrounding LP, including LGd, LD, PO, LH, and APN were drawn first and are indicated with different color lines. **B**, **E**, and **H** depict the subsequent addition of LP in solid pink. **C**, **F**, and **I** show the projections in LP from TEa (127089669) at the approximate corresponding coronal, sagittal, and horizontal planes to the average template. The projections labeled by EGFP are in green. Because sagittal and horizontal views are off-axis reconstructions of the experimental coronal blockface images, they are noticeably softer in clarity. The shape of LP drawn in coronal, sagittal, and horizontal planes on the average template is well-matched with the TEa injection. Abbreviations: APN, anterior pretectal nucleus; LD, lateral dorsal nucleus of thalamus; LGd, dorsal part of the lateral geniculate complex; LH, lateral habenula; LP, lateral posterior nucleus of the thalamus; PO, posterior complex of the thalamus; *R*, rostral; *L*, lateral.

Table 1. Structures delineated in 3-D for the mouse CCF.

Id	Name	Acronym	Large Brain Region
353	Primary somatosensory area, nose	SSp-n	Isocortex
329	Primary somatosensory area, barrel field	SSp-bfd	Isocortex
337	Primary somatosensory area, lower limb	SSp-ll	Isocortex
345	Primary somatosensory area, mouth	SSp-m	Isocortex
369	Primary somatosensory area, upper limb	SSp-ul	Isocortex
361	Primary somatosensory area, trunk	SSp-tr	Isocortex
182305689	Primary somatosensory area, unassigned	SSp-un	Isocortex
1002	Primary auditory area	AUDp	Isocortex
402	Anterolateral visual area	VISal	Isocortex
394	Anteromedial visual area	VISam	Isocortex
409	Lateral visual area	VISl	Isocortex
385	Primary visual area	VISp	Isocortex
425	Posterolateral visual area	VISpl	Isocortex
533	posteromedial visual area	VISpm	Isocortex
312782546	Anterior area	VISa	Isocortex
312782574	Laterointermediate area	VISli	Isocortex
417	Rostrolateral visual area	VISrl	Isocortex
312782628	Postrhinal area	VISpor	Isocortex
894	Retrosplenial area, lateral agranular part	RSPagl	Isocortex
879	Retrosplenial area, dorsal part	RSPd	Isocortex
886	Retrosplenial area, ventral part	RSPv	Isocortex
507	Main olfactory bulb	MOB	Olfactory areas
188	Accessory olfactory bulb, glomerular layer	AOBgl	Olfactory areas
196	Accessory olfactory bulb, granular layer	AOBgr	Olfactory areas
204	Accessory olfactory bulb, mitral layer	AOBmi	Olfactory areas
1139	Nucleus of the lateral olfactory tract, layer 3	NLOT3	Olfactory areas
382	Field CA1	CA1	Hippocampal formation
423	Field CA2	CA2	Hippocampal formation
463	Field CA3	CA3	Hippocampal formation
10703	Dentate gyrus, molecular layer	DG-mo	Hippocampal formation
10704	Dentate gyrus, polymorph layer	DG-po	Hippocampal formation
632	Dentate gyrus, granule cell layer	DG-sg	Hippocampal formation
982	Fasciola cinerea	FC	Hippocampal formation
502	Subiculum	SUB	Hippocampal formation
583	Claustrum	CLA	Cortical subplate
952	Endopiriform nucleus, dorsal part	EPd	Cortical subplate
131	Lateral amygdalar nucleus	LA	Cortical subplate
303	Basolateral amygdalar nucleus, anterior part	BLAa	Cortical subplate
311	Basolateral amygdalar nucleus, posterior part	BLAp	Cortical subplate
672	Caudoputamen	CP	Striatum
56	Nucleus accumbens	ACB	Striatum
754	Olfactory tubercle	OT	Striatum
250	Lateral septal nucleus, caudal (caudodorsal) part	LSc	Striatum
333	Septohippocampal nucleus	SH	Striatum
1022	Globus pallidus, external segment	GPe	Pallidum
1031	Globus pallidus, internal segment	GPi	Pallidum

287	Bed nucleus of the anterior commissure	BAC	Pallidum
629	Ventral anterior-lateral complex of the thalamus	VAL	Thalamus
685	Ventral medial nucleus of the thalamus	VM	Thalamus
718	Ventral posterolateral nucleus of the thalamus	VPL	Thalamus
733	Ventral posteromedial nucleus of the thalamus	VPM	Thalamus
1044	Peripeduncular nucleus	PP	Thalamus
475	Medial geniculate complex	MG	Thalamus
170	Dorsal part of the lateral geniculate complex	LGd	Thalamus
218	Lateral posterior nucleus of the thalamus	LP	Thalamus
1020	Posterior complex of the thalamus	PO	Thalamus
325	Suprageniculate nucleus	SGN	Thalamus
255	Anteroventral nucleus of thalamus	AV	Thalamus
127	Anteromedial nucleus	AM	Thalamus
64	Anterodorsal nucleus	AD	Thalamus
155	Lateral dorsal nucleus of thalamus	LD	Thalamus
1113	Interanterodorsal nucleus of the thalamus	IAD	Thalamus
1120	Interanteromedial nucleus of the thalamus	IAM	Thalamus
59	Intermediodorsal nucleus of the thalamus	IMD	Thalamus
362	Mediodorsal nucleus of thalamus	MD	Thalamus
366	Submedial nucleus of the thalamus	SMT	Thalamus
149	Paraventricular nucleus of the thalamus	PVT	Thalamus
15	Parataenial nucleus	PT	Thalamus
181	Nucleus of reunions	RE	Thalamus
189	Rhomboid nucleus	RH	Thalamus
907	Paracentral nucleus	PCN	Thalamus
575	Central lateral nucleus of the thalamus	CL	Thalamus
599	Central medial nucleus of the thalamus	CM	Thalamus
930	Parafascicular nucleus	PF	Thalamus
262	Reticular nucleus of the thalamus	RT	Thalamus
27	Intergeniculate leaflet of the lateral geniculate complex	IGL	Thalamus
178	Ventral part of the lateral geniculate complex	LGv	Thalamus
321	Subgeniculate nucleus	SubG	Thalamus
483	Medial habenula	MH	Thalamus
186	Lateral habenula	LH	Thalamus
390	Supraoptic nucleus	SO	Hypothalamus
338	Subfornical organ	SFO	Hypothalamus
210	Lateral mammillary nucleus	LM	Hypothalamus
491	Medial mammillary nucleus	MM	Hypothalamus
470	Subthalamic nucleus	STN	Hypothalamus
797	Zona incerta	ZI	Hypothalamus
851	Superior colliculus, optic layer	SCop	Midbrain
842	Superior colliculus, superficial gray layer	SCsg	Midbrain
4	Inferior colliculus	IC	Midbrain
381	Substantia nigra, reticular part	SNr	Midbrain
26	Superior colliculus, motor related, deep gray layer	SCdg	Midbrain
42	Superior colliculus, motor related, deep white layer	SCdw	Midbrain
17	Superior colliculus, motor related, intermediate white layer	SCiw	Midbrain
10	Superior colliculus, motor related, intermediate gray layer	SCig	Midbrain

795	Periaqueductal gray	PAG	Midbrain
215	Anterior pretectal nucleus	APN	Midbrain
214	Red nucleus	RN	Midbrain
35	Oculomotor nucleus	III	Midbrain
115	Trochlear nucleus	IV	Midbrain
757	Ventral tegmental nucleus	VTN	Midbrain
12	Interfascicular nucleus raphe	IF	Midbrain
100	Interpeduncular nucleus	IPN	Midbrain
612	Nucleus of the lateral lemniscus	NLL	Pons
7	Principal sensory nucleus of the trigeminal	PSV	Pons
122	Superior olivary complex, periolivary region	POR	Pons
105	Superior olivary complex, medial part	SOCm	Pons
114	Superior olivary complex, lateral part	SOCl	Pons
880	Dorsal tegmental nucleus	DTN	Pons
931	Pontine gray	PG	Pons
318	Supragenual nucleus	SG	Pons
574	Tegmental reticular nucleus	TRN	Pons
621	Motor nucleus of trigeminal	V	Pons
679	Superior central nucleus raphe	CS	Pons
147	Locus ceruleus	LC	Pons
207	Area postrema	AP	Medulla
96	Dorsal cochlear nucleus	DCO	Medulla
101	Ventral cochlear nucleus	VCO	Medulla
711	Cuneate nucleus	CU	Medulla
1039	Gracile nucleus	GR	Medulla
903	External cuneate nucleus	ECU	Medulla
642	Nucleus of the trapezoid body	NTB	Medulla
429	Spinal nucleus of the trigeminal, caudal part	SPVC	Medulla
437	Spinal nucleus of the trigeminal, interpolar part	SPVI	Medulla
445	Spinal nucleus of the trigeminal, oral part	SPVO	Medulla
653	Abducens nucleus	VI	Medulla
661	Facial motor nucleus	VII	Medulla
576	Accessory facial motor nucleus	ACVII	Medulla
939	Nucleus ambiguus, dorsal division	AMBd	Medulla
143	Nucleus ambiguus, ventral division	AMBv	Medulla
1048	Gigantocellular reticular nucleus	GRN	Medulla
83	Inferior olivary complex	IO	Medulla
136	Intermediate reticular nucleus	IRN	Medulla
106	Inferior salivatory nucleus	ISN	Medulla
203	Linear nucleus of the medulla	LIN	Medulla
852	Parvicellular reticular nucleus	PARN	Medulla
169	Nucleus prepositus	PRP	Medulla
209	Lateral vestibular nucleus	LAV	Medulla
202	Medial vestibular nucleus	MV	Medulla
225	Spinal vestibular nucleus	SPIV	Medulla
1041	Paraflocculus	PFL	Cerebellum
1049	Flocculus	FL	Cerebellum
989	Fastigial nucleus	FN	Cerebellum

91	Interposed nucleus	IP	Cerebellum
846	Dentate nucleus	DN	Cerebellum
1016	olfactory nerve layer of main olfactory bulb	onl	Fiber tracts
665	lateral olfactory tract, body	lot	Fiber tracts
900	anterior commissure, olfactory limb	aco	Fiber tracts
848	optic nerve	IIn	Fiber tracts
117	optic chiasm	och	Fiber tracts
125	optic tract	opt	Fiber tracts
158	posterior commissure	pc	Fiber tracts
911	trochlear nerve	IVn	Fiber tracts
93	motor root of the trigeminal nerve	moV	Fiber tracts
794	spinal tract of the trigeminal nerve	sptV	Fiber tracts
798	facial nerve	VIIn	Fiber tracts
413	vestibular nerve	vVIIIn	Fiber tracts
633	inferior colliculus commissure	cic	Fiber tracts
697	medial lemniscus	ml	Fiber tracts
237	solitary tract	ts	Fiber tracts
326	superior cerebelar peduncles	scp	Fiber tracts
78	middle cerebellar peduncle	mcp	Fiber tracts
1123	inferior cerebellar peduncle	icp	Fiber tracts
728	arbor vitae	arb	Fiber tracts
776	corpus callosum	cc	Fiber tracts
784	corticospinal tract	cst	Fiber tracts
6	internal capsule	int	Fiber tracts
924	cerebal peduncle	cpd	Fiber tracts
1092	external medullary lamina of the thalamus	em	Fiber tracts
190	pyramid	py	Fiber tracts
908	anterior commissure, temporal limb	act	Fiber tracts
940	cingulum bundle	cing	Fiber tracts
603	fimbria	fi	Fiber tracts
436	columns of the fornix	fx	Fiber tracts
449	ventral hippocampal commissure	vhc	Fiber tracts
443	dorsal hippocampal commissure	dhc	Fiber tracts
690	mammilothalmic tract	mtt	Fiber tracts
802	stria medullaris	sm	Fiber tracts
595	fasciculus retroflexus	fr	Fiber tracts
611	habenular commissure	hbc	Fiber tracts
81	lateral ventricle	VL	Ventricular systems
129	third ventricle	V3	Ventricular systems
140	cerebral aqueduct	AQ	Ventricular systems
145	fourth ventricle	V4	Ventricular systems
153	lateral recess	V4r	Ventricular systems
164	central canal, spinal cord/medulla	c	Ventricular systems

REFERENCES

Dong HW (2008) *Allen Reference Atlas: a digital color brain atlas of the C57BL/6J male mouse*. Hoboken, NJ: John Wiley & Sons.

Fonov V, Evans AC, Botteron K, Almli CR, McKinstry RC, Collins DL (2011) Brain Development Cooperative Group. Unbiased average age-appropriate atlases for pediatric studies. *Neuroimage* 54:313-327.

Garrett ME, Nauhaus I, Marshel JH, Callaway EM (2014) Topography and areal organization of mouse visual cortex. *Journal Neuroscience* 34:12587-12600.

Kuan L, Li Y, Lau C, Feng D, Bernard A, Sunkin SM, Zeng H, Dang C, Hawrylycz M, Ng L (2015) Neuroinformatics of the Allen Mouse Brain Connectivity Atlas. *Methods* 73:4-17.

Lein ES, Callaway EM, Albright TD, Gage FH (2005) Redefining the boundaries of the hippocampal CA2 subfield in the mouse using gene expression and 3-dimensional reconstruction. *Journal Comparative Neurology* 485:1-10.

Lein ES, Hawrylycz MJ, Ao N, Ayres M, Bensinger A, Bernard A, Boe AF, Boguski MS, Brockway KS, Byrnes EJ, Chen L, Chen L, Chen TM, Chin MC, Chong J, Crook BE, Czaplinska A, Dang CN, Datta S, Dee NR, Desaki AL, Desta T, Diep E, Dolbeare TA, Donelan MJ, Dong HW, Dougherty JG, Duncan BJ, Ebbert AJ, Eichele G, Estin LK, Faber C, Facer BA, Fields R, Fischer SR, Fliss TP, Frensley C, Gates SN, Glattfelder KJ, Halverson KR, Hart MR, Hohmann JG, Howell MP, Jeung DP, Johnson RA, Karr PT, Kawal R, Kidney JM, Knapik RH, Kuan CL, Lake JH, Laramee AR, Larsen KD, Lau C, Lemon TA, Liang AJ, Liu Y, Luong LT, Michaels J, Morgan JJ, Morgan RJ, Mortrud MT, Mosqueda NF, Ng LL, Ng R, Orta GJ, Overly CC, Pak TH, Parry SE, Pathak SD, Pearson OC, Puchalski RB, Riley ZL, Rockett HR, Rowland SA, Royall JJ, Ruiz MJ, Sarno NR, Schaffnit K, Shapovalova NV, Sivisay T, Slaughterbeck CR, Smith SC, Smith KA, Smith BI, Sodt AJ, Stewart NN, Stumpf KR, Sunkin SM, Sutram M, Tam A, Teemer CD, Thaller C, Thompson CL, Varnam LR, Visel A, Whitlock RM, Wohnoutka PE, Wolkey CK, Wong VY, Wood M, Yaylaoglu MB, Young RC, Youngstrom BL, Yuan XF, Zhang B, Zwingman TA, Jones AR (2007) Genome-wide atlas of gene expression in the adult mouse brain. *Nature* 445:168-176.

Marshel JH, Garrett ME, Nauhaus I, Callaway EM (2011) Functional specialization of seven mouse visual cortical areas. *Neuron* 72:1040–1054.

Oh SW, Harris JA, Ng L, Winslow B, Cain N, Mihalas S, Wang Q, Lau C, Kuan L, Henry AM, Mortrud MT, Ouellette B, Nguyen TN, Sorensen SA, Slaughterbeck CR, Wakeman W, Li Y, Feng D, Ho A, Nicholas E, Hirokawa KE, Bohn P, Joines KM, Peng H, Hawrylycz MJ, Phillips JW, Hohmann JG, Wohnoutka P, Gerfen CR, Koch C, Bernard A, Dang C, Jones AR, Zeng H (2014) A mesoscale connectome of the mouse brain. *Nature* 508:207-214.

Paxinos G, Franklin KBJ (2001) *The Mouse Brain in Stereotaxic Coordinates*, Second edition. Elsevier Academic Press, San Diego, CA.

Ragan T, Kim KH, Bahlmann, K, So PT (2004) Two-photon Tissue Cytometry. *Methods in Cell Biology* 75:23-39.

Ragan T, Sylvan JD, Kim KH, Huang H, Bahlmann K, Lee RT, So PT (2007) High-resolution whole organ imaging using two-photon tissue cytometry. *J Biomedical Optics* 12:014015.

Wang Q, Burkhalter A (2007) Area map of mouse visual cortex. *Journal Comparative Neurology* 502:339-357.

Wang Q, Gao E, Burkhalter A (2011) Gateways of ventral and dorsal streams in mouse visual cortex. *Journal Neuroscience* 31:1905-1918.

Yushkevich PA, Piven J, Hazlett HC, Smith RG, Ho S, Gee JC, Gerig G (2006) User-guided 3D active contour segmentation of anatomical structures: Significantly improved efficiency and reliability. *Neuroimage* 31:1116-1128.